Ocean temperature variability for the past 60 years on the Norwegian-Svalbard margin influences gas hydrate stability on human time scales

Bénédicte Ferré,[1] Jürgen Mienert,[1] and Tomas Feseker[2]

Received 20 June 2012; revised 11 September 2012; accepted 12 September 2012; published 23 October 2012.

[1] The potential impact of future climate change on methane release from oceanic gas hydrates is the subject of much debate. We analyzed World Ocean Database quality controlled data on the Norwegian-Svalbard continental margin from the past 60 years to evaluate the potential effect of ocean temperature variations on continental margin gas hydrate reservoirs. Bottom water temperatures in the Norwegian-Svalbard margin were subject to significant cooling until 1980 (by ~2°C offshore NW-Svalbard and in the Barents Sea) followed by a general bottom water temperature increase until 2010 (~0.3°C in deep-water areas offshore NW-Svalbard and mid-Norwegian margin and ~2°C in the shallow areas of the Barents Sea and Prins Karls Forland). Bottom water warming in the shallow outer shelf areas triggered the Gas Hydrate Stability Zone (GHSZ) retreat toward upper continental slope areas, potentially increasing methane release due to gas hydrate dissociation. GHSZ responses to temperature changes on human time scales occur exclusively in shallow water and only if near-surface gas hydrates exist. The responses are associated with a short time lag of less than 1 year. Temperatures in the bottom water column seem to be partly regulated by the North Atlantic Oscillation (NAO), with positive NAO associated with warm phases. However, cooling events in the surface water offshore NW-Svalbard might be associated with El Niño events of 1976–1977, 1986–1987 and 1997–1998 in the Pacific. Such ocean cooling, if long enough, may delay ocean temperature driven gas hydrate dissociation and potential releases of methane to the ocean.

Citation: Ferré, B., J. Mienert, and T. Feseker (2012), Ocean temperature variability for the past 60 years on the Norwegian-Svalbard margin influences gas hydrate stability on human time scales, *J. Geophys. Res.*, *117*, C10017, doi:10.1029/2012JC008300.

1. Introduction

[2] It is evident through observations over the past decades that climate change is occurring [e.g., *Antoniades et al.*, 2011; *Vinther et al.*, 2009; *Graversen et al.*, 2008]. However, how these changes will affect the oceanic, atmospheric and terrestrial environments is still unclear. Natural changes to climate have occurred in the past, but the rapid increase in global temperatures in recent decades (i.e., +0.6°C in the last three decades) [*Hansen et al.*, 2010] suggests that the dominant factor driving climate change is linked to human influence, mainly through emission of carbon dioxide and other greenhouse gases [*Jain*, 1993; *Intergovernmental Panel on Climate Change* (*IPCC*), 2007]. Warming of both atmospheric and oceanic temperatures is predicted to be greater in the Norwegian-Svalbard region compared to other locations at similar latitudes, mainly due to the warming of inflowing Atlantic Water [e.g., *Spielhagen et al.*, 2011] and reduction of sea ice cover [*Screen and Simmonds*, 2010] . Such warming of ocean temperatures is expected to reduce the stability of gas hydrates in continental margins [e.g., *Mienert et al.*, 2005].

[3] Gas hydrate is a crystalline solid consisting of gas molecules, usually methane, each surrounded by a cage of water molecules [*Sloan*, 1990]. Gas hydrates occur abundantly in nature, particularly in Arctic regions. Evidence of free gas accumulation beneath gas hydrate accumulation is inferred from the presence of a cross-cutting, polarity-reversed, high-amplitude bottom-simulating reflector (BSR) that marks the base of the gas hydrate stability zone (GHSZ) [e.g., *Shipley et al.*, 1979; *Mienert and Posewang*, 1999] (Figure 1). Gas hydrate builds-up in the pore space of sediments and may create a caprock preventing the escape of free gas to the seabed. Hydrate formation is favored at high pressure and low temperature [*Sloan*, 1998], indicating a high potential for the abundance of gas hydrates beneath the seafloor along continental margins and permafrost areas. Estimates of the global gas hydrate reservoir suggest large quantities of gas, spanning from 82×10^{11} m^3 to 46×10^{15} m^3 [*MacDonald*, 1990; *Kvenvolden*, 1988; *Ginsburg and Soloviev*, 1995; *Harvey and Huang*,

[1]Institute of Geology, University of Tromsø, Tromsø, Norway.
[2]MARUM—Center for Marine Environmental Sciences and Faculty of Geosciences, University of Bremen, Bremen, Germany.

Corresponding author: B. Ferré, Institute of Geology, University of Tromsø, NO-9037 Tromsø, Norway. (benedicte.ferre@uit.no)

0148-0227/12/2012JC008300

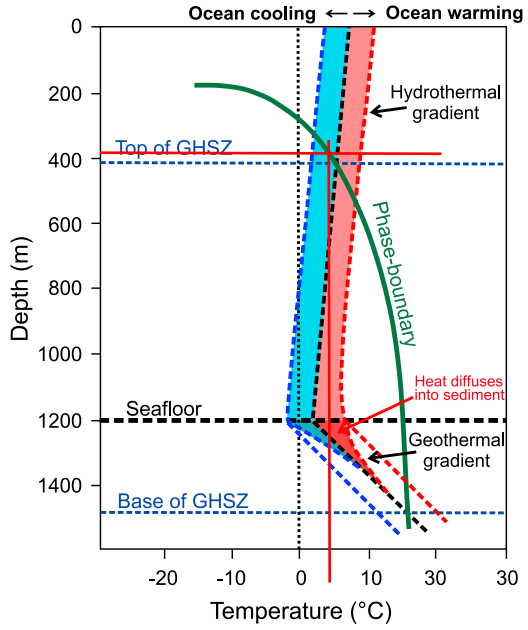

Figure 1. Sketch of the stability field for methane hydrate [*Sloan*, 1990] in the water column and sub seabed. Heat from ocean-bottom water warming diffuses into the seabed causing a reduction of the gas hydrate stability zone. The average depth of the GHSZ is calculated from the temperature at the seafloor and the geothermal gradient, here considered to be 30°C/km.

1995; *Milkov*, 2004; *Archer et al.*, 2009; *Boswell and Collett*, 2011; *Burwicz et al.*, 2011], estimates which we expect to be revised with time. Gas hydrates can cause environmental changes through decomposition, which may destabilize sediments and cause slope instabilities [e.g., *Mienert et al.*, 2005]. The vast amount of methane that emanates from gas hydrates can have a significant impact on ocean chemistry and global warming if it reaches the atmosphere [*Blunier et al.*, 1995]. Moreover, gas hydrates are also a potential unconventional energy resource [*Boswell and Collett*, 2011].

[4] Many studies have already demonstrated the effect of warming in the Arctic, with significant sea ice retreat, glacier melting [*Rignot and Kanagaratnam*, 2006] and release of methane [*Shakhova et al.*, 2010], a major greenhouse gas which can enhance ocean acidification through oxidization of methane to CO_2 in the water column [*Biastoch et al.*, 2011]. Melting ice sheets due to warmer ocean temperatures have also been linked to increases in earthquake frequency [*Turpeinen et al.*, 2008], which can also result in the release of shallow gas hydrates from the seabed.

[5] The objective of the present study is to analyze World Ocean Database quality controlled data from the last 60 years to evaluate the potential effect and the sensitivity of ocean temperature variations on gas hydrate reservoirs of the Norwegian-Svalbard continental margin.

2. Working Areas

[6] The Norwegian-Svalbard continental margin extends from 60°N to 80°N with water depths ranging from 350 m in the western Barents Sea to 3800 m along the continental margin offshore Svalbard (Figure 2). The continental margin is highly dynamic, with abundant evidence of fluid migration processes [*Hustoft et al.*, 2009a], submarine sliding [*Mienert and Weaver*, 2003; *Vorren et al.*, 1998] and the presence of gas hydrates [*Vogt et al.*, 1999; *Mienert et al.*, 1998; *Andreassen and Hansen*, 1995]. Here we focus on locations where gas hydrate reservoirs have been identified: the Storegga Slide at the mid-Norwegian margin, the Barents Sea trough and North–Western (NW) Svalbard continental margin (Figure 2).

[7] The Storegga slide event occurred approximately 8250 years ago [*Haflidason et al.*, 2004], involving the displacement of 3500 km^3 of sediment [*Bryn et al.*, 2003] that caused a 10–12 m high tsunami wave at the west coast of

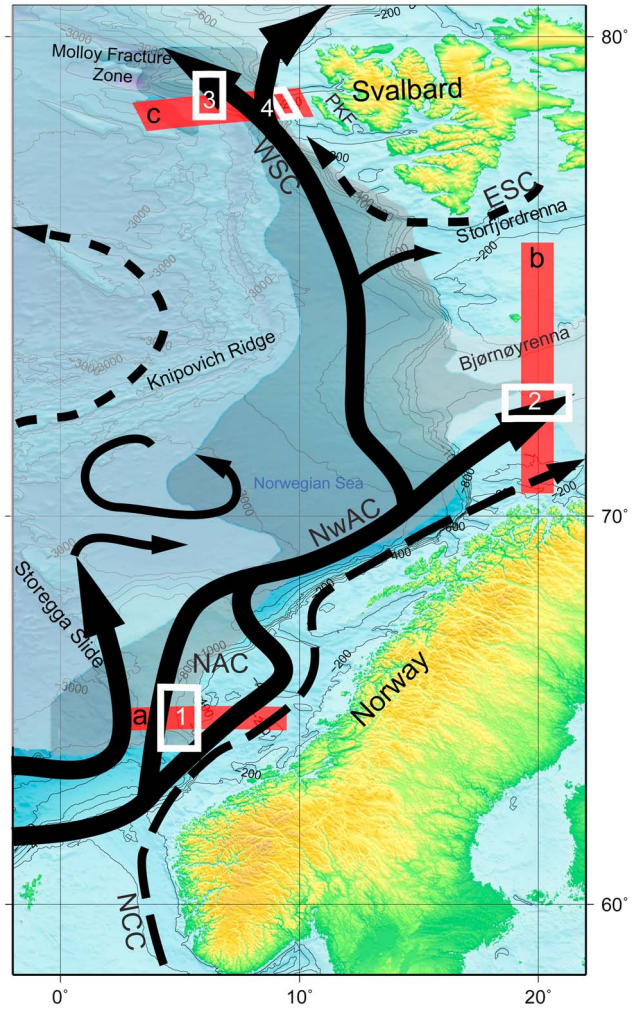

Figure 2. General map of the area. Potential equilibrium between pure-methane hydrate and fresh water (light gray) and highest potential for existence of gas hydrate (dark gray) are represented [*Andreassen and Hansen*, 1995]. Red shaded areas a, b, c indicate the location of the profiles in Figure 5, and white squares numbered 1 to 4 show the locations of time series in Figure 6. PKF stands for Prins Karls Forland. Black arrows represent the warm branches from the Atlantic current and dotted arrows show the cold branches from the Arctic current. Dashed arrow is the coastal current.

Norway [*Bondevik et al.*, 2003]. Overpressure due to rapid sediment loading, gas release from decomposition of gas hydrate and earthquakes are the most probable causes for creating weak sediment layers, enabling slope failures in the area [*Mienert et al.*, 2005; *Bryn et al.*, 2003]. Pockmark fields have been detected between 700 m and 900 m water depth at Nyegga just north of the Storegga Slide [*Bünz et al.*, 2003, *Hustoft et al.*, 2009a] (section a and area 1 in Figure 2). Modeling of the GHSZ showed that hydrate stability is considerably more sensitive to temperature variations than to sea level variations (pressure changes), especially at shallower depths [*Mienert et al.*, 2005].

[8] In contrast to the mid-Norwegian margin area, the northern region of the Barents Sea is a large epi-continental sea and is bordered to the west and north by young passive continental margins [*Faleide et al.*, 1984]. The bathymetry in the Barents Sea comprises a major cross-shelf trough (Bjørnøyrenna or Bear Island Trough) reaching 500 m water depth, and a shallower bank to the north reaching 350 m water depth, with another trough (Storfjordrenna) (Figure 2). Gas hydrates were inferred by identification of a BSR in the Bjørnøyrenna area, at a bottom depth between 300 and 350 m [*Andreassen et al.*, 1990] (section b and area 2 in Figure 2) located near seabed crater fields that were most likely caused by gas blow-outs [*Solheim and Elverhøi*, 1985]. This area has been strongly influenced by ice sheet loading or reloading and sea level and bottom water temperature changes, thus distinctly influencing the depth of the gas hydrate stability zone [e.g., *Mienert and Posewang*, 1999].

[9] The NW-Svalbard continental margin (section c in Figure 2) includes several fields of gas hydrate and active methane release [*Hustoft et al.*, 2009b; *Vanneste et al.*, 2005; *Mienert and Posewang*, 1999; *Andreassen and Hansen*, 1995]. The gas hydrate fields represent an area of active fluid escape associated with characteristic pockmarks concentrating on the crest of the Vestnesa sediment drift located at water depths between 1120 and 1450 m (area 3 in Figure 2) [*Hustoft et al.*, 2009b; *Vogt et al.*, 1994]. More recently, shallow water areas of NW-Svalbard (area 4 in Figure 2) showed evidence for several hundred gas flares (acoustic expression of methane bubbles emanating from the seabed) between 150 and 400 m water depth [*Knies et al.*, 2004; *Westbrook et al.*, 2009; *Rajan et al.*, 2012]. Flares are located eastward of the upper limit of the GHSZ along the continental margin [*Westbrook et al.*, 2009; *Rajan et al.*, 2012]. The flares have heights of more than 270 m and some may reach the sea surface [*Westbrook et al.*, 2009]. However, *Fisher et al.* [2011] did not detect any oceanic gas hydrate related methane anomalies reaching the atmosphere. Methane may reach the atmosphere if significant releases resulting from warming of shallow subsurface sediments and gas hydrates occur [*Krey et al.*, 2009]. Such observations exist from the East Siberian Arctic Shelf where estimates showed a positive flux of CH_4 venting to the atmosphere from shallow water of ~45 m [*Shakhova et al.*, 2010].

[10] In terms of ocean circulation, the North Atlantic Current (NAC) is the northern extension of the Gulf Stream and brings warm and saline waters in the area to form the Norwegian Atlantic Current (NwAC) (Figure 2). One branch continues to the North and forms the West Spitsbergen Current (WSC) while the other branch follows the coast of Norway toward the shallow Barents Sea. The Norwegian Coastal Current (NCC) proceeds from north of Scotland and continues along the Norwegian coast and into the Barents Sea. The East Spitsbergen Current (ESC) carries Arctic Water to the west toward the WSC, creating a front at the shelf break [*Schlichtholz and Goszczko*, 2006] (Figure 2).

3. Methods

3.1. WOD Data and Quality Control

[11] The World Ocean Database (WOD) covers more than 2 centuries of ocean temperature and salinity data. The latest version (WOD09) was downloaded from http://www.nodc.noaa.gov/OC5/indprod.html. Data that failed quality control were removed based on range assessment for 28 ocean areas at 33 standard levels [*Boyer et al.*, 2009]. The present study includes CTD (Conductivity Temperature and Depth) data over the past 60 years. Only data from May to September were taken to avoid seasonal variation and misinterpretation due to unequal number of measurements. Indeed, more data are available during summer months and this is likely due to preferable ship operational sea conditions during this time of the year. Temperature and salinity data were interpolated using the DIVA Gridding method of the Ocean Data View software (R. Schlitzer, 2011, available at http://odv.awi.de), and averaged over the 60 years (from 1 January 1950 to 31 December 2009) to provide an overview of the water masses in each section a to c (Figure 2). A total of 816 CTD profiles were available in section a (mid-Norwegian margin), 4835 in section b (Barents Sea) and 839 in section c (NW-Svalbard). Temperature and salinity time series profiles focus at the depth range of pockmarks, which are considered as the most sensitive methane release areas (areas 1 to 4 in Figure 2). A total of 209 CTD profiles were available in area 1 (mid-Norwegian margin), 413 in area 2 (Barents Sea), 171 in area 3 (NW-Svalbard) and 253 in area 4 (Prins Karls Forland) which provide the necessary resolution for comparisons. The bottom water temperature values represent the yearly average in the first 10% above the seabed.

3.2. Calculation of the Hydrate Stability Zone

[12] The extent of the GHSZ in the sub-seafloor at a given gas composition depends on water depth, bottom water temperature, geothermal gradient and to a smaller extent, salinity [*Sloan*, 1990]. As most submarine gas hydrates are formed by methane, this study focuses on the physical parameters that limit the stability field of pure methane hydrates. Within the GHSZ, however, methane hydrates occur only if the pore water is oversaturated with methane. As methane concentrations in the pore water were neglected in this study, the estimates of the extent of the GHSZ represent merely the volumes of sediment in which methane hydrates could occur in case of methane oversaturation. Figure 1 illustrates the hydrate stability curve, represented by the boundary between free methane gas and methane hydrate for seawater obtained from the compilation of *Sloan* [1990]. This curve illustrates that gas hydrates are stable at high pressure (deep water) and low temperature. Consequently, the extent of the GHSZ may decrease with increasing bottom water temperature but increase with increasing sea level rise (increasing pressure), which may counteract the influence of ocean warming (Figure 1).

[13] In order to determine the evolution of bottom water temperature along transect lines, water temperature near the seabed along the sections a to c has been calculated in and around areas where hydrate has been previously detected using geophysical methods. CTD measurements within the first 10% of water column above the seabed have been averaged. In case the bottom depth was not available from the CTD data at a particular site, we used the averaged bottom depth from adjacent CTD casts to take the best available value for the corresponding temperature/salinity. For each transect, a temperature grid was interpolated in time and space using a kriging algorithm with automatic parameter estimation provided by the software "intamap" (E. Pebesma et al., intamap: Procedures for automated interpolation, R package version 1.3–4, 2010, available at http://CRAN.R-project.org/package=intamap) in R [*R Development Core Team*, 2010]. The temporal resolution of all three grids was 1 year. The spatial resolution of the grids was 1, 2 and 0.5 km for the transect lines across the Storegga area at the mid-Norwegian margin (section a), the Barents Sea (section b) and NW-Svalbard margin (section c), respectively. Transects across the mid-Norwegian and Svalbard margins comprised a large depth interval (from 150 to 2000 m depth in mid-Norwegian margin and from 50 to 2600 m depth in the Svalbard margin). As bottom water temperature generally decreases with increasing water depth, a linear relationship between temperature and depth was assumed and universal kriging was applied to remove this trend from the data set. In contrast, the North–South orientation of a transect across the Barents Sea resulted in a clearly visible trend from higher temperatures at lower latitudes to lower temperatures at higher latitudes. This trend was removed from the data set and ordinary kriging was applied to the residuals.

[14] The transient exchange of heat between the bottom water and the sediment was modeled using a semianalytical approach described by *Carslaw and Jaeger* [1959]. The change in sediment temperature ΔT in response to a change in bottom water temperature ΔT_{bw} is given by

$$\Delta T(z,t) = \Delta T_{bw} \cdot \mathrm{erfc}\left(\frac{z}{2\sqrt{\kappa t}}\right)$$

where z is the sediment depth, t is the time since the change in bottom water temperature took effect, and κ is the thermal diffusivity of the sediment. If the evolution of the bottom water temperature is defined as a series of yearly mean values, the changes in sediment temperature are given by

$$\begin{aligned}\Delta T(z,i) = {} & \Delta T_{bw,1} \cdot \mathrm{erfc}\left(\frac{z}{2\sqrt{\kappa \cdot 31536000\,s}}\right) \\ & + \Delta T_{bw,2} \cdot \mathrm{erfc}\left(\frac{z}{2\sqrt{\kappa \cdot 31536000\,s}}\right) \\ & + \ldots + \Delta T_{bw,i} \cdot \mathrm{erfc}\left(\frac{z}{2\sqrt{\kappa \cdot 31536000\,s}}\right)\end{aligned}$$

where $\Delta T_{bw,i}$ is the change in bottom water temperature between the years i-1 and i. At the start of the simulations, the temperature profiles were linear and in equilibrium with the corresponding bottom water temperature. The initial temperature gradient and the thermal conductivity along the modeled transect lines were estimated based on in situ temperature gradient and thermal conductivity measurements available from the Global Heat Flow Database of the International Heat Flow Commission (see http://www.heatflow.und.edu/). Thermal conductivity was then converted to thermal diffusivity using an empirical relationship proposed by *Von Herzen and Maxwell* [1959]:

$$\kappa = (3.656788 \times K - 0.7) \times 10^{-7}$$

where K is the thermal conductivity in W/(m °C) and the thermal diffusivity κ is in m/s^2.

[15] For the mid-Norwegian and NW-Svalbard margins, all temperature gradient measurements located within 100 km from the transect lines were projected onto the transect lines. Only two measurements in the Global Heat Flow Database were located near the transect line across the Barents Sea. Based on these values, a constant initial temperature gradient of 38°C/km and a constant thermal diffusivity of around 4.68×10^{-7} m/s^2 were used for the entire transect.

[16] The temperature gradient measurements near the mid-Norwegian transect show a median of 65°C/km [e.g., *Vogt and Sundvor*, 1996] with locally increased values on the upper slope (Figure 3a). Possible explanations for these local heat flow highs were discussed by *Vogt and Sundvor* [1996]. The temperature gradients may reach median values beyond the local high. Figure 3b shows measured values of thermal conductivity ranging between 0.77 and 1.36 W/(m °C). This illustrates a trend from low values at the deep end to high values at the shallow end of the transect profile. This may indicate an increase in grain size toward the shore, which will increase the thermal conductivity [e.g., *Midttomme and Roaldset*, 2008].

[17] As illustrated in Figure 3c, geothermal gradient measurements near the transect line across the Svalbard margin range between 65 and 460°C/km and show a trend from higher values close to the ocean ridge (deep water) to lower values at the shelf (shallow water). As this trend reflects the cooling of the oceanic crust with increasing distance from the mid-ocean ridge, it becomes clear that the temperature gradient is at its minimum at the shallow end of the transect profile. Inversely, the values of measured thermal conductivity increase from around 1 W/(m °C) at the deep water to more than 1.6 W/(m °C) at the shallow end of the transect profile (Figure 3d), corresponding most probably to an increase in grain sizes, analogous to the transect across the mid-Norwegian margin.

[18] Water depths along the transect lines were taken from the *GEBCO*08 bathymetry (version 27 September 2010, see http://www.gebco.net) and converted to pressure according to *Saunders* [1981], using the mean latitudes of each transect line. Assuming hydrostatic pressure in the subseafloor and using the mean bottom water salinity of each transect, the dissociation temperature of pure methane hydrates was calculated as a function of depth following the Pitzer approach [*Tishchenko et al.*, 2005]. For each year, the GHSZ was determined as the section of the sedimentary column in which the modeled sediment temperature was below the dissociation temperature.

[19] The median of the kriging standard deviation of the bottom water temperature was around 0.8°C for all three grids (Figures 4c, 4g, and 4k). This value reflects the variability of the bottom water temperature inherent in the data

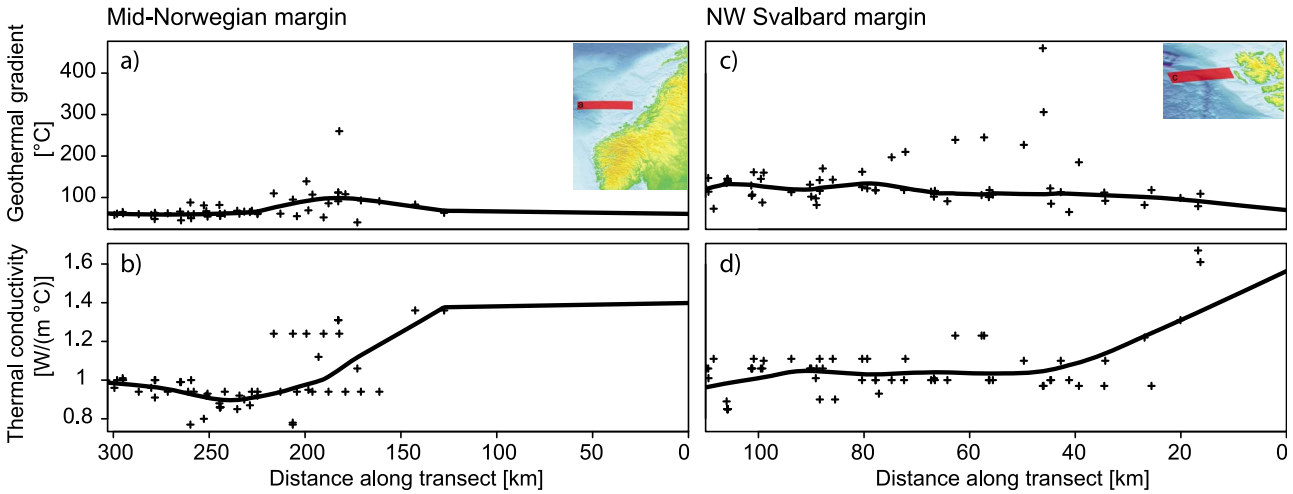

Figure 3. Geothermal gradient and thermal conductivity along the transect lines across the mid-Norwegian and Svalbard margins. The crosses indicate measured values extracted from the Global Heat Flow Database of the International Heat Flow Commission (see http://www.heatflow.und.edu/). The lines show the values used for the initial geothermal gradient and for calculating the thermal diffusivity along the transect lines a and c (Figure 2).

sets, which limits the precision of the interpolated temperature grids. Higher standard deviations of up to 1.44°C occurred in those parts of the grids where the data coverage was poor. The highest standard deviation of nearly 1.9°C occurred within a limited area on the upper slope of the Svalbard transect and is most likely related to high variability of the CTD measurements (Figure 4k).

4. Results

4.1. Oceanography

[20] The northward currents (NAC, NwAC and WSC; Figure 2) carry the North Atlantic Water (NAW) above 700 m depth along the Norwegian and Svalbard continental margins into the Arctic (Figures 5 and 6). During this path, NAW changes significantly through mixing with colder/fresher water and heat loss to atmosphere [*Piechura et al.*, 2001]. In this study, NAW is associated with salinities higher than 35 Practical Salinity Unit (PSU) and temperatures higher than 2°C offshore the NW-Svalbard margin [*Swift and Aagaard*, 1981] (Figures 5c, 6c, and 6d) and higher than 6°C at the mid-Norwegian margin [*Haugan et al.*, 1991] (Figures 5a, 5b, 6a, and 6b). Norwegian Sea Arctic Intermediate Water (NSAIW) flows below NAW and reaches down to 1000 m, with temperatures from −0.5 to 0.5°C and salinity between 34.87 and 34.90 PSU [*Hansen and Østerhus*, 2000] (Figures 5a, 5c, 6a, and 6c). The Norwegian Sea Deep Water (NSDW) has the greatest density, with temperatures less than −0.5°C and salinities around 34.91 PSU [*Hansen and Østerhus*, 2000] (Figures 5a, 5c, 6a, and 6c). The Norwegian Coastal Water (NCW) carried by NCC flows above NAW on the Norwegian margin (Figure 5a), whereas the Arctic Water (ArW) is carried by ESC above NAW on the NW-Svalbard margin (Figures 5b, 5c, and 6d). The NCW is colder (2 to 6°C) and fresher (average of 34.5 PSU) than NAW due to water coming from the brackish Baltic Sea as well as the Norwegian fjords and rivers [*Sætre*, 1999]. The ArW is also colder (<3°C) and fresher (<34.4 PSU) than NAW due to ice melting as well as fjord and river inputs. Distribution of NAW and ArW in the Barents Sea highlights the presence of a Polar Front following approximately the 250 m isobaths around Bjørnøyrenna Trough [*Harris et al.*, 1998] (Figure 5b).

4.2. Temperature Variations and Evolution of the GHSZ

[21] The results of the bottom water temperature interpolation using the kriging algorithm and the modeled evolution of the GHSZ for all three transects are illustrated in Figure 4. The variability of the volume of the GHSZ and its upper limit at the seafloor along the three transects is summarized in Table 1. Figure 7 shows a comparison of the variability of the GHSZ and the interpolated bottom water temperature above the GHSZ at water depths of less than 500 m.

4.2.1. Mid-Norwegian Margin

[22] At the mid-Norwegian margin (section a in Figure 2), the interpolated in situ ocean temperature data were averaged between 1950 and 2010 (Figure 5a), and showed −0.60 ± 0.46°C in the first 10% above the pockmark area (orange line on the seabed between 700 and 900 m depth including 1288 bottom water temperature (BWT) measurements). However, bottom water temperature time series in the area 1 (blue line in Figure 6a) shows a strong variability before 1987 (average of −0.86 ± 0.13°C, 89 BWT measurement) followed by a steady temperature increase up to −0.31 ± 0.10°C until 2009 (939 BWT measurements). The time trend of ocean temperature and salinity between 700 and 900 m water depth in area 1 highlights two temperature and salinity anomalies that are clearly evident in the years 2000 and 2007 (Figure 6a).

[23] The initial pressure and temperature conditions along the mid-Norwegian transect permit the existence of gas hydrates at water depths below 485 m (Figure 4a). Between 1952 and 1990, the mean bottom water temperature above the entire GHSZ decreased from around 0.69°C to around

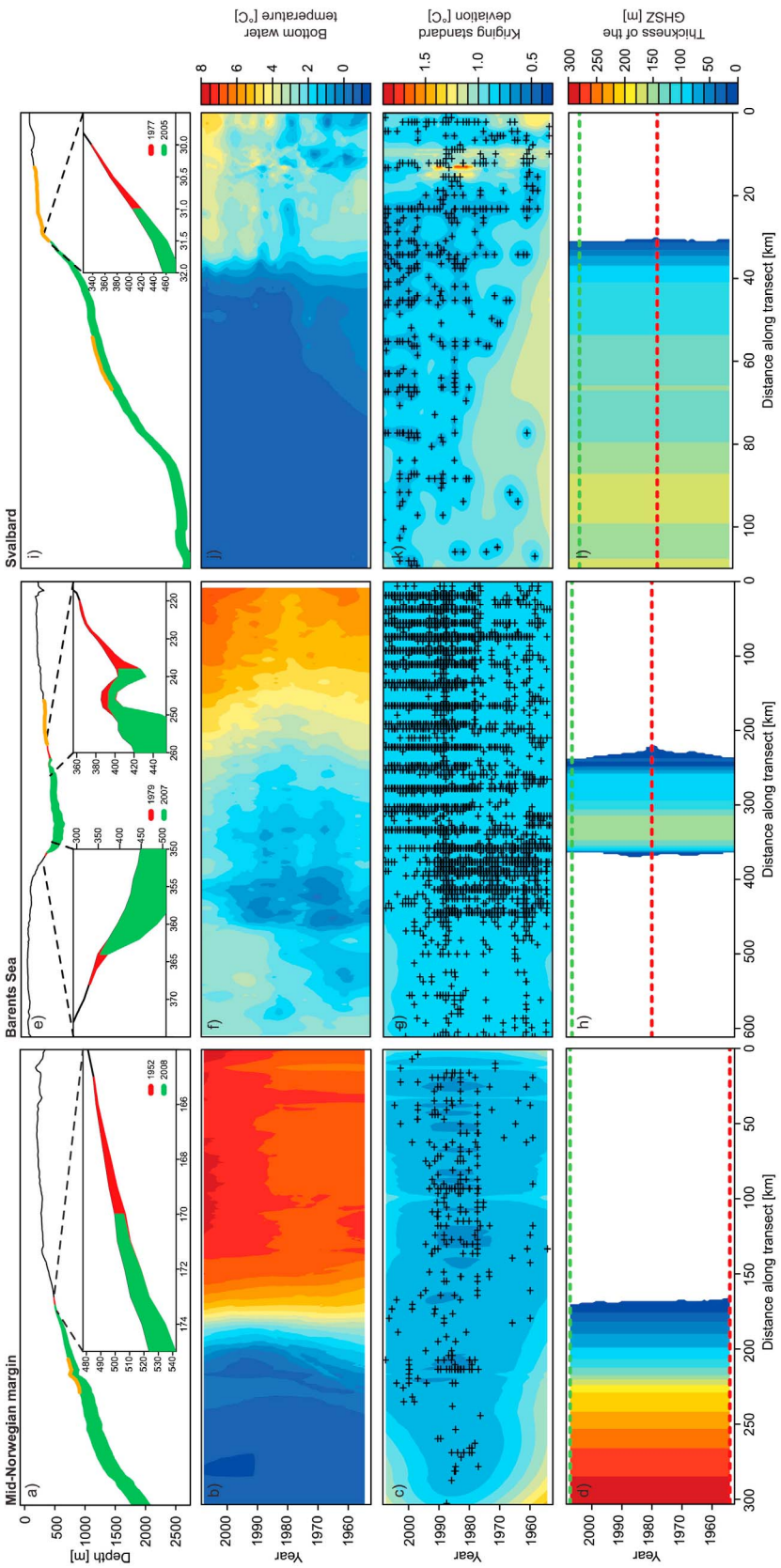

Figure 4. (a, e, and i) Bathymetry and maximum extent of the GHSZ, (b, f, and j) evolution of bottom water temperature, (c, g, and k) kriging standard deviation with crosses indicating the measurements, and (d, h, and l) evolution of the thickness of the GHSZ along the transect lines. Small figures inside the top row show the comparison of the minimum (green) and maximum (red) extents of the GHSZ for each transect at the indicated year and orange thick segments represent the areas where pockmarks/gas hydrate exist.

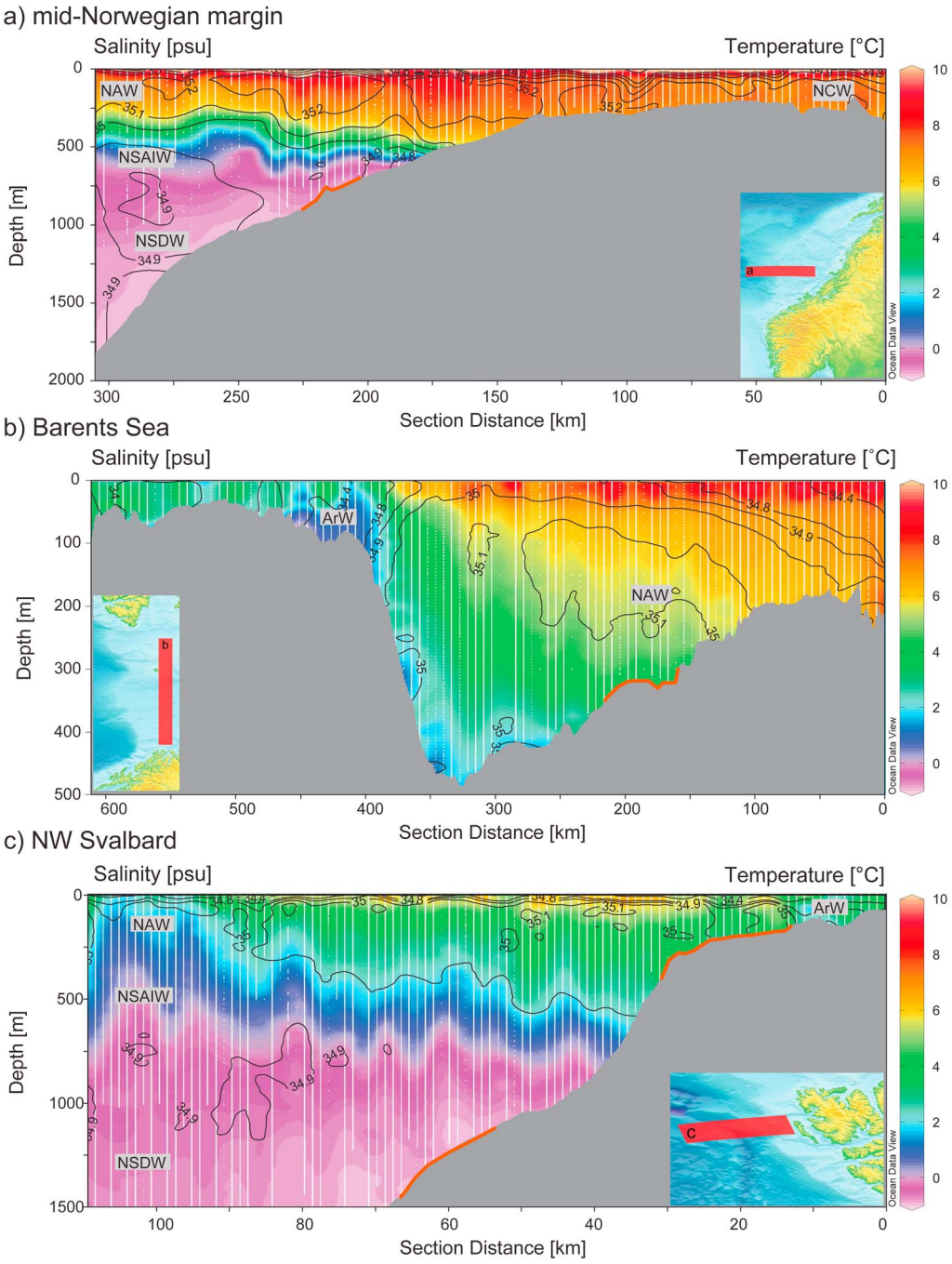

Figure 5. Temperature and salinity time series profiles along the sections in red shaded section a to c, averaged between 1950 and 2010. Acronyms for water masses are detailed in the text. White dots are the CTD locations and orange lines on the seabed represent the areas where pockmarks/gas hydrate exist.

0.17°C (Figure 4b). After 1990, the bottom water temperature started to increase more and more rapidly and reached its maximum around 0.42°C at the end of the time period covered by the presented data. It is noteworthy that the initial decrease of the bottom water temperature does not lead to a significant increase in the volume of the GHSZ (Figure 4d). Above the shallow GHSZ at less than 500 m water depth, the bottom water temperature evolution opposed the initial cooling trend: between 1952 and 1962, the bottom water temperature above the shallow hydrates increased from 5.05°C to 5.29°C, which was accompanied by a retreat of the GHSZ (Figure 7). The bottom water temperature above the shallow GHSZ then continued to increase gradually to 5.39°C in 1994 and more rapidly to 5.63°C at the end of the time period covered by the data presented here. The evolution of the volume of the GHSZ along the transect line mirrors the evolution of the bottom water temperature above the shallow GHSZ. Short-term decreases in mean temperature by less than 0.1°C around 1967 and 1997 are followed by equally short-term increases in the volume of the GHSZ

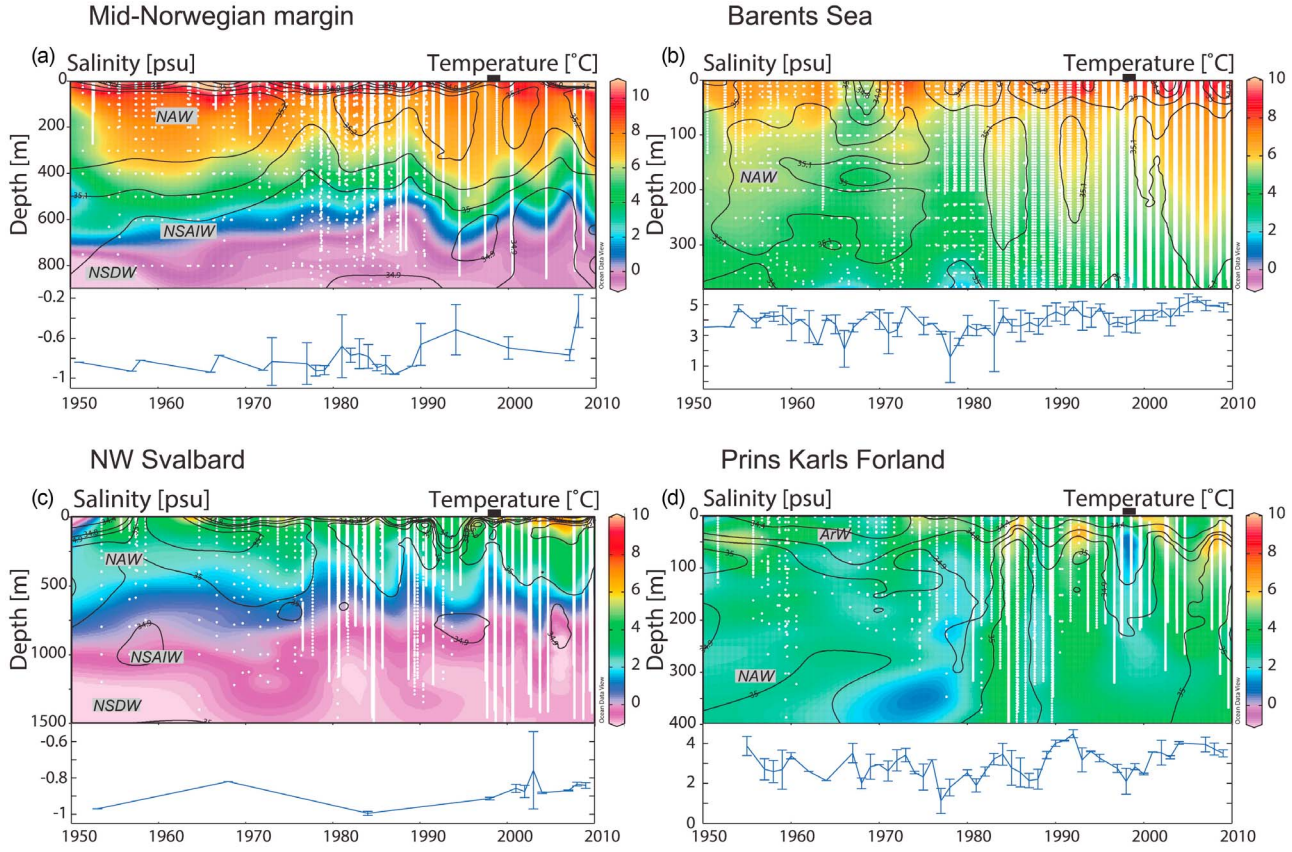

Figure 6. Temperature and salinity time series in the white squares 1 to 4 in Figure 2: (a) square 1, (b) square 2, (c) square 3, and (d) square 4. Acronyms for water masses are detailed in the text. Blue line is the bottom water temperature in the first 10% above the seabed, white dots are the locations of the CTD profiles, and black segment highlight the 1997–1998 El Niño event.

by around 1700 to 3000 m^3/m with a time lag of 1 year, which indicates that the shallow GHSZ at the mid-Norwegian margin responds relatively quickly to changes in bottom water temperature (Figure 7). In total, the volume of the GHSZ decreased by 15 046 m^3/m between 1952 and 2008 (Table 1).

4.2.2. Barents Sea

[24] In the Barents Sea (section b in Figure 2), bottom water temperature was averaged between 1950 and 2010 in the first 10% above the seabed and showed values of 3.67 ± 1.31°C where geophysical evidence for gas hydrate exists (area 2 in Figure 2 and orange line on the seabed in Figure 5b includes 2638 BWT measurements). Time series of temperature and salinity profiles in the water column above potential gas hydrate areas highlight a deepening of the NAW from 1980 with a slight cooling early 1998, followed by a rapid warming and a deepening of the warmer water masses (Figure 6b). Bottom water temperature in the first 10% above the seabed (blue line in Figure 6b) first shows a slow decrease with a rate of −0.03°C/yr until 1978 (77 BWT measurements), followed by an increase with a rate of 0.06°C/yr (2321 BWT measurements) leading to relatively warm temperatures of 4.8 ± 0.29°C in 2009 (includes 110 BWT measurements).

[25] The initial conditions along the transect line across the Barents Sea favor the formation of gas hydrates at water depths of less than 386 m in the southern part and less than 350 m in the northern part (Figure 4e). Between 1950 and 1966, the mean bottom water temperature above the GHSZ decreased from around 2.2°C to 1.6°C (Figure 4f), which caused an increase in the volume of the GHSZ by about 48 640 m^3/m until 1965, accompanied by an advance of its upper limit to water depths of up to 374 m in the south and 329 m in the north (Figure 4h). Due to the gentle slope in the

Table 1. Variability of the GHSZ Along the Three Transect Lines (Figure 2)

	Mid-Norwegian Margin	Barents Sea	Svalbard
Depth of upper limit of GHSZ at seafloor	485–500 m	317–375 m (N) 363–404 m (S)	338–438 m
Horizontal variability of upper limit at seafloor	5 km	8 km (N) and 20 km (S)	1.5 km
Variability in volume of GHSZ	15,046 m^3 per m	149,616 m^3 per m	2783 m^3 per m

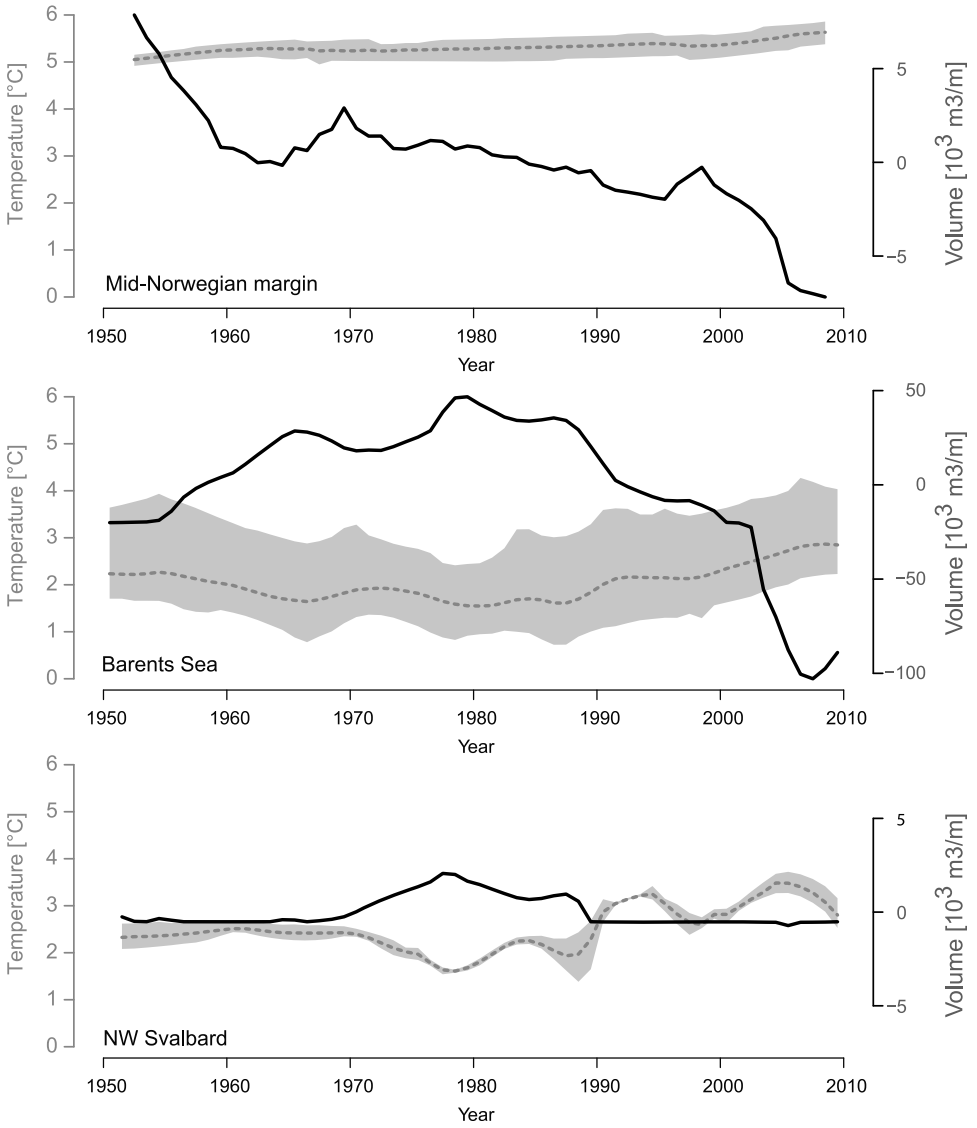

Figure 7. Variability of the volume of the GHSZ (black) compared to the evolution of bottom water temperature (gray) above the GHSZ at less than 500 m water depth. For each transect, the volume of the GHSZ was normalized by subtracting the mean.

southern part of the transect line, this corresponds to a horizontal shift of 8 km, compared to 4 km in the north. The initial temperature decrease was followed by a short-term increase to 1.93°C in 1972, before the temperature dropped to its minimum of 1.55°C in 1980. The GHSZ responded to this short-term increase in bottom water temperature with a decrease in volume of about 11 300 m^3/m. After 1980, the mean bottom water temperature above the GHSZ rose rapidly to 2.87°C in 2008, interrupted by short-term decreases by about 0.1°C in 1987 and by about 0.03°C in 1997. These short-term temperature decreases coincide with minor and very short-term increases in volume of the GHSZ by around 2000 m^3/m in 1986 and around 200 m^3/m in 1997. The mean bottom water temperature reached its maximum value of 2.87°C in 2008 and decreased again by around 0.2°C in 2009. In total, the evolution of the volume of the GHSZ varied by 149 616 m^3/m during the time period covered by the data (Table 1).

4.2.3. NW-Svalbard

[26] At the NW-Svalbard continental margin (section c in Figure 2), the average bottom water temperature in the first 10% above the deep-water pockmark areas (area 3 and orange line in deeper part in Figure 5c, 3281 BWT measurements) is -0.77 ± 0.34°C. Three cooling events occurred in the deep-water area in 1977, 1987 and 1998, and a short-term warming event occurred in 2003 (Figure 6c). The 60 year bottom temperature time series shows a temperature increase from -0.99 ± 0.01°C in 1984 (191 BWT measurements) to -0.84 ± 0.02°C in 2009 (160 BWT measurements), with a slow rate of 0.007°C/yr (blue line in Figure 6c). In contrast, the shallow area with abundant gas flares (area 4 and orange line from 150 to 400 m depth in Figure 5c, 1037 BWT measurements) shows an average bottom temperature in the first 10% above the seabed of 2.65 ± 1.13°C. The shallow area shows a bottom water temperature trend that is negative until 1978 with a rate of −0.03°C/yr, followed by a positive

trend with a rate of 0.05°C/yr. Four ocean warming events (temperature increased by ~2°C) occurred in the shallow area (area 4) in 1985, 1992, 2003 and 2007, and four ocean cooling events (temperature decreased by ~3°C) occurred in 1975, 1977, 1987 and 1998 (Figure 6d).

[27] Under initial conditions of the simulation, gas hydrates are stable at water depths deeper than 369 m (Figure 4i). The bottom water temperature above the entire GHSZ decreased from −0.08°C in 1951 to −0.58°C in 1981, with a short-term maximum of around −0.26°C in 1970 (Figure 4j). However, bottom water temperature above the shallow GHSZ stagnated at around 2.42°C until 1970 (Figure 4j), so that the volume of the GHSZ remained constant during this period of time in spite of the overall bottom water temperature decrease (Figure 4l). After 1970, the cooling trend reached the bottom water above the shallow GHSZ and leads to a decrease in mean temperature to 1.61°C until 1978. At the same time, the volume of the GHSZ reaches its maximum of 2 261 m^3/m above the initial volume (Figure 4l). This is accompanied by an expansion of the GHSZ to water depths of up to 338 m (Table 1). From 1978 until the end of the time period covered by the data, the bottom water temperature increased by around 0.008°C/yr above the entire GHSZ and by around 0.048°C/yr above the shallow GHSZ. This general trend was interrupted by short-term cooling in 1987, 1998, and toward the end of the time series. These quasiperiodic cooling events were characterized by temperature decreases on the order of 0.05°C above the entire GHSZ and 1 order of magnitude larger above the shallow GHSZ. The temperature minimum in 1987 coincides with a short-term increase in the volume of the GHSZ of approximately 300 m^3/m. After reaching this peak value, the volume of the GHSZ decreases rapidly back to its initial value and stagnates until the end of the time period covered by the data. Minor cooling events that followed afterward are not accompanied by significant changes in the volume of the GHSZ. This suggests that the amplitude of the bottom water temperature fluctuations is too small to affect a significant area of the margin. Due to the steep slope at the Svalbard margin, the shifts of the upper limit of the GHSZ in response to these temperature changes translate to horizontal distances of less than the distance between two neighboring grid points (500 m).

[28] The kriging interpolation of the bottom water temperature evolution along the transect lines clearly reveals different trends for the deep (>500 m) and shallow water (<500 m) areas of the transects. Between 1950 and 1980, the deep-water transects across the mid-Norwegian and Svalbard margins were subject to significant bottom water cooling, while the shallow-water transect showed no significant changes or increases in bottom water temperature above GHSZ. After 1980, the Svalbard margin showed bottom water warming in both the deep and shallow water transects above the GHSZ. Noteworthy, bottom water warming in the shallower areas was 1 order of magnitude more rapid than above the deep areas above the GHSZ.

5. Discussion

5.1. Temperature Variation

[29] Significant variations in atmospheric temperature have been observed over the past century. Modeling of temperature with and without addition of anthropogenic effect demonstrated that warming prior to 1970 was due to natural variation, whereas increased warming after this period was mainly attributed to anthropogenic greenhouse gases (i.e., CO_2) [*Hegerl et al.*, 2007]. However, in the Arctic, an important cooling event was observed from 1940 to 1970 followed by a warming [*Chylek et al.*, 2009], which is consistent with the cooling observed in our presented bottom water data at the Norwegian and Svalbard continental margins (Figures 4 (second row) and 6). *Chylek et al.* [2009] suggested that the Atlantic Multidecadal Oscillation (AMO) was mainly responsible for Arctic temperature variations, implying a role of the global thermohaline circulation in Arctic temperature variations. The North Atlantic Oscillation (NAO) is another important phenomenon to take into consideration, as it influences the temperature and current of the entire North Atlantic [*Hurrell*, 1995; *Hurrell et al.*, 2001]. A positive (negative) NAO phase is associated with increased (diminished) Icelandic Low and Azores High as well as intensified (reduced) westerly winds across the Atlantic. During the positive phase, southwesterly winds are intensified over the Norwegian and Barents Sea, carrying warm air masses and causing warm Atlantic water flow to the northern areas [*Blindheim et al.*, 2000]. Focusing on the presented time range from 1950 to 2010, temporal evolution of the NAO in winter (December to March) highlights the most extreme negative indexes until the 1960s, followed by persistent positive indexes from the late 1980s/early 1990s until now [*Dickson et al.*, 2000; *Stenseth et al.*, 2003]. All time series exhibited increasing ocean temperatures from 1980, supporting the influence of a positive NAO (Figures 4 (second row) and 6). Yearly averaged bottom water temperature and temperature grid calculated with the kriging method highlighted that this phenomenon affected the entire water column down to at least 1500 m water depth. This trend is even more pronounced offshore Prins Karls Forland (Figure 6d), where the warm/colder cycles of bottom water temperatures from 1980 follow the NAO winter (3 year running averaged) trend (data courtesy of Climatic Research Unit, University of East Anglia, http://www.cru.uea.ac.uk/cru/data/nao/nao.dat), with a correlation coefficient of 0.68. However, the NAO index cannot explain all the trends in the investigated transect areas.

[30] El Niño is a global ocean-atmosphere phenomenon occurring on average every 5 years in the Pacific Ocean. This event causes warming of ocean currents along the coasts of Peru and Ecuador, and is connected with dramatic changes in the weather patterns in this region. Two strong El Niño events occurred in 1982–1983 and 1997–1998, the last one being the most powerful event over the past 50 years [*Sidorova and Shcherbinin*, 2009]. Although these events are known to affect vast regions of the tropics, Pacific and Indian Ocean and the surrounding landmasses, their influence can be felt in the Polar Regions. *Sidorova and Shcherbinin* [2009] studied the effect of the 1997–1998 El Niño event in the Barents Sea hydrodynamics, and found a decrease of supply of warm and saline North Atlantic Waters triggering an abnormally cold northern winter a few months after the event was recorded in the Pacific. Time series in the Barents Sea and offshore Svalbard (Figure 6b to 6d) show a sudden and isolated cooling (up to 5°C from ~6 to ~1°C) in the upper 500 m of the water column in 1998, highlighting the

possibility that the same event affected the Svalbard margin and the Barents Sea.

[31] *Bjerknes* [1966] attributed temperature anomalies in Europe to the El Niño event that occurred in 1957–1958. Unfortunately, the present study cannot reveal any particular trends occurring during that time period due to lack of available data. However, El Niño events that occurred in the winters of 1976–1977 and 1986–1987 might explain the cooling by ~1°C offshore Svalbard (Figures 4j, 6c, and 6d).

5.2. Hydrate Stability Zone Evolution

[32] Ocean warming on the upper slopes has a greater effect on the extent of the GHSZ than downslope because the GHSZ shoals with increasing bottom water temperatures and decreasing pressure [*Mienert et al.*, 2005]. Moreover, methane hydrate dissociation on the upper slope is controlled by ocean warming, whereas it is more controlled by sea level changes in the deeper basin where ocean temperatures remain low.

[33] Measurements taken from the Global Heat Flow Database indicated that the thermal conductivity of the sediments along the transect lines across the mid-Norwegian and Svalbard margins increases landward, which allowed temperature changes in the bottom water to propagate more rapidly into the sediment column toward the shelf areas. The scarcity of available heat flow measurements in the Barents Sea region prevented an assessment of changes in geothermal gradients and thermal conductivity, and inevitably resulted in a poorly constrained model. However, we cannot see any geological reason to assume significant variations in background geothermal gradient or thermal conductivity along the transect line across the Barents Sea, particularly since the GHSZ is limited to the central part of the transect.

[34] The modeling of the response of the GHSZ to changes in bottom water temperature indicates the sensitivity of shallow water gas hydrate fields to global warming (Figure 4, bottom row). Particularly at the transect across the Barents Sea, the changes in bottom water temperature resulted in strongly nonlinear temperature profiles, which caused the GHSZ to shrink both at the bottom and at the top as the bottom water temperature increased (Figure 4h). The short-term bottom temperature decreases in 1987 and 1997–1998 are associated with short-term increases in the volume of the GHSZ in the Barents Sea, but only the 1987 cooling event affected the volume of the GHSZ in NW-Svalbard and only the 1997–1998 event affected the volume of the GHSZ in the mid-Norwegian margin.

[35] The initial conditions assumed that the sediment temperature profile was linear and in equilibrium with the bottom water temperature at the start of all three simulations. Depending on the thermal conductivity, the sediment depth, and the magnitude of the changes in bottom water temperature, it takes several years to decades until realistic temperature profiles evolve during the simulations. Earlier studies linking observed gas emissions to the dissociation of gas hydrates assumed continuous steady state conditions and a linear increase in bottom water temperature [e.g., *Westbrook et al.*, 2009], providing maximum retreats in the extent of the GHSZ. However, ocean bottom water temperature changes and its penetration into the seabed are much more complex and follow time-dependent transient changes. The semianalytical approach followed here described transient changes in sediment temperature driven by yearly measurements. If shallow gas hydrates exist in the pore space of sediments, the propagation of a heat pulse into the sediment will be delayed by the consumption of latent heat during gas hydrate dissociation. Inversely, the cooling of sediment may be delayed by heat production during gas hydrate formation. More recent studies [e.g., *Reagan and Moridis*, 2009] have attempted to use very advanced numerical models that include phase changes as well as multiphase flow to explain gas emissions observed in gas hydrate fields. However, the quality of the model results depends on detailed information on the distribution and concentration of gas hydrate in the pore space of sediment that is seldom available.

[36] At least for the transects across the mid-Norwegian and Svalbard margins, the total volume of the GHSZ depended on the length of the transect profile and was thus arbitrary. However, as distinct changes in the GHSZ related to ocean temperature can be expected in more shallow water areas upslope, the variability in volume can be compared by subtracting the mean from the time series for each transect. Normalized in this way, the changes in volume along the transect lines across the mid-Norwegian and Svalbard margins are in the same order of magnitude, while the variability of the GHSZ volume along the transect profile across the Barents Sea was 1 order of magnitude higher (Figure 7 and Table 1). The largest changes in volume occurred in the Barents Sea, which comprises two shallow areas of the GHSZ. The combination of shallow water depth and a gentle slope resulted in a very large horizontal variability of the upper limit of the GHSZ (Table 1). Along the transect profile across the mid-Norwegian margin, both the horizontal variability of the upper limit and the changes in volume were intermediate, while the smallest changes in volume occurs along the transect line across the Svalbard margin (Table 1).

[37] Information regarding the recession of the uppermost limit of the GHSZ at the seafloor is important as this process might cause a significant release of methane from melting of oceanic hydrates (Figure 8). In a shallow slope region like the Barents Sea, a large area of the seabed could be affected. The stability curve (Figure 1) illustrates that gas hydrates can be found in very shallow water depths of up to 150 m if temperatures are below 0°C [*Kvenvolden*, 1993]. For this reason, Polar Regions represent one of the main gas hydrate formation regions but also one of the most sensitive regions for ocean temperature [*Mienert and Posewang*, 1999]. A temperature increase of only 1°C on the upper continental margins (<1000 m depth) would be enough for the gas hydrate to migrate completely out of the stability field and potentially release methane into the ocean and possibly to the atmosphere.

[38] Although the GHSZ is especially sensitive to temperature increases in the Arctic, gas hydrates under the warm Gulf stream areas of the NE Atlantic margins are as well particularly susceptible to release methane if ocean warming occurs. Adding to the complexity of potential gas hydrate dissociation and methane release, we consider four simple scenarios concentrating only on geological and ocean temperature controls in polar margins (Figure 8). Scenario I shows warm water in contact with the seabed causing a penetration of the warm pulse into the seabed. The related melting of existing gas hydrate layers occurs at the most upper continental slope and is associated with an increased methane release from the seabed into the ocean. Scenario II involves geological controls on gas hydrate formation in

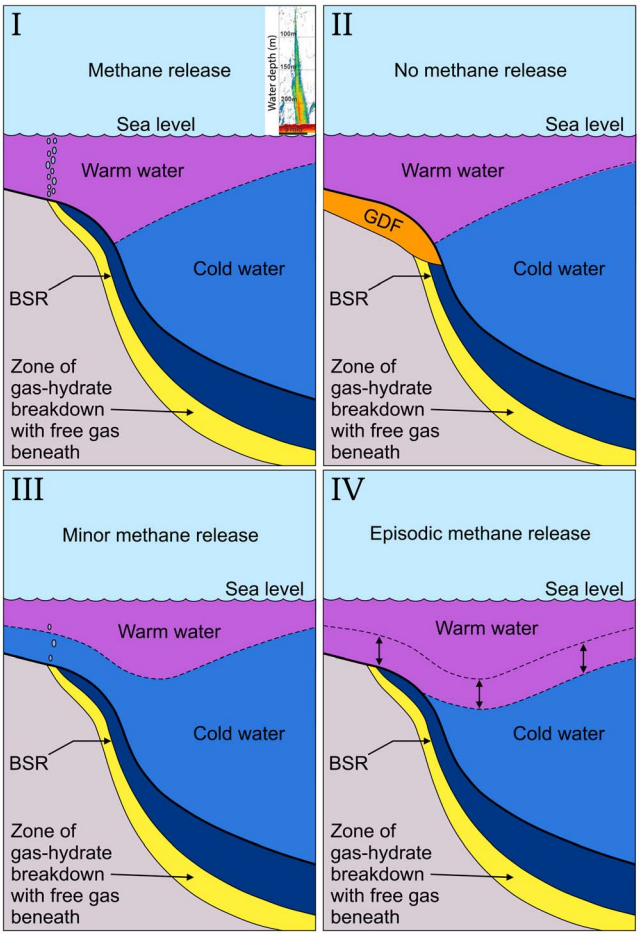

Figure 8. Scenarios of hydrate dissociation and methane release controlled by geology and temperature warming. GDF in scenario II stands for Glacigenic debris flows. An example of an acoustic gas flare measured with a 38 kHz echosounder profile (*R/V* Jan Mayen cruise in the area off Prins Karls Forland (area 4, July 2009) is shown in scenario I. The different scenarios are explained in the text.

form of dense material such as glacigenic debris flows (GDFs), less permeable and known to hinder gas hydrate formation and thus gas release [e.g., *Bünz et al.*, 2003]. The impact of ocean warming on the gas hydrate field that is draped by GDFs bears no significance if compared to scenario I. Scenario III shows a situation in which ocean warming does not reach the seabed and thus does not cause perturbation of the geothermal gradient. If any methane release occurs, it should not be related to gas hydrate dissociation and ocean temperature. Scenario IV suggests episodic methane release due to the fact that water masses of increased (decreased) temperature in contact with the seabed to cause a disturbance of the geothermal gradients and thus methane (no methane) release due to gas hydrate (or no) dissociation.

6. Conclusion

[39] Sixty years of quality controlled data from the World Ocean Database at the Norwegian-Svalbard continental margin highlights the distinction between shallow and deep-water areas, where the effect of ocean temperature variation on gas hydrate reservoirs depends on a continued climate warming at contemporary rates over long time scales (>100 years).

[40] Gas hydrates stability zone responses to temperature changes on human time scales occur exclusively in shallow water depth and are associated with a very short time lag (<1 year). In all three depth transect profiles, the GHSZ retreats toward lower continental slope regions due to increasing bottom temperature at upper continental slopes (>500 m depth). The Barents Sea represents the largest volume change in the GHSZ. Solid proof is still lacking that gas hydrate dissociation contributes to major seepage from upper continental slopes.

[41] The influence of a positive North Atlantic Oscillation (NAO) is illustrated in both data and model simulations by a warming since the 1980s down to at least 1500 m depth, due to transport of Atlantic Water northward driven by southwesterly winds. Short-term cooling events in the first 500 m offshore Svalbard might be associated with El Niño events occurring in the Pacific in the winters 1976–1977, 1986–1987 and 1997–1998.

[42] **Acknowledgments.** We thank the NODC/NOAA for providing the in situ temperature and salinity data from the World Ocean Database. This data set is available from the Web page http://www.nodc.noaa.gov/OC5/SELECT/dbsearch/dbsearch.html. This work was supported by EC funding from the Seventh Framework program (FP7) EMSO (European Multidisciplinary Seafloor Observatory) and SIOS (Svalbard Integrated Arctic Earth Observing System).

References

Andreassen, K., and T. Hansen (1995), Inferred gas hydrates offshore Norway and Svalbard, *Norw. J. Geol.*, *45*, 10–34.

Andreassen, K., K. Hogstad, K. A. Berteussen (1990), Gas hydrate in the southern Barents Sea, indicated by a shallow seismic anomaly, *First Break*, *8*(6), 235–245, doi:10.3997/1365-2397.1990012.

Antoniades, D., P. Francus, R. Pienitz, G. St-Onge, and W. F. Vincent (2011), Holocene dynamics of the Arctic's largest ice shelf, *Proc. Natl. Acad. Sci. U. S. A.*, *108*, 1–6, doi:10.1073/pnas.1106378108.

Archer, D., B. Buffett, and V. Brovkin (2009), Ocean methane hydrates as a slow tipping point in the global carbon cycle, *Proc. Natl. Acad. Sci. U. S. A.*, *106*(49), 20,596–20,601, doi:10.1073/pnas.0800885105.

Biastoch, A., et al. (2011), Rising Arctic Ocean temperatures cause gas hydrate destabilization and ocean acidification, *Geophys. Res. Lett.*, *38*, L08602, doi:10.1029/2011GL047222.

Bjerknes, J. (1966), A possible response of the atmospheric Hadley circulation to equatorial anomalies of ocean temperature, *Tellus*, *18*(4), 820–829, doi:10.1111/j.2153-3490.1966.tb00303.x.

Blindheim, J., V. Borovkov, B. Hansen, S. A. Malmberg, W. R. Turrell, and S. Østerhus (2000), Upper layer cooling and freshening in the Norwegian Sea in relation to atmospheric forcing, *Deep Sea Res. Part I*, *47*(4), 655–680, doi:10.1016/S0967-0637(99)00070-9.

Blunier, T., J. Chappellaz, J. Schwander, B. Stauffer, and D. Raynaud (1995), Variations in atmospheric methane concentration during the Holocene epoch, *Nature*, *374*, 46–49, doi:10.1038/374046a0.

Bondevik, S., J. Mangerud, S. Dawson, A. Dawson, and Ø. Lohne (2003), Record-breaking height for 8000-year-old tsunami in the North Atlantic, *Eos Trans. AGU*, *84*(31), 289, doi:10.1029/2003EO310001.

Boswell, R., and T. S. Collett (2011), Current perspectives on gas hydrate resources, *Energy Environ. Sci.*, *4*, 1206–1215, doi:10.1039/c0ee00203h.

Boyer, T. P., et al. (2009), *World Ocean Database 2009*, *NOAA Atlas NESDIS*, vol. 66, 216 pp., NOAA, Silver Spring, Md.

Bryn, P., A. Solheim, K. Berg, R. Lien, C. F. Forsberg, H. Haflidason, D. Ottensen, and L. Rise (2003), The Storegga Slide complex: Repeated large scale sliding in response to climatic cyclicity, in *Submarine Mass Movements and Their Consequences. Advances in Natural and Technological Hazards Research*, edited by J. Locat and J. Mienert, pp. 215–222, Kluwer Acad., Dordrecht, Netherlands, doi:10.1007/978-94-010-0093-2_24.

Bünz, S., J. Mienert, and C. Berndt (2003), Geological controls on the Storegga gas-hydrate system of the mid-Norwegian continental margin, *Earth Planet. Sci. Lett.*, *209*(3–4), 291–307, doi:10.1016/S0012-821X(03)00097-9.

Burwicz, E. B., L. H. Rüpke, and K. Wallmann (2011), Estimation of the global amount of submarine gas hydrates formed via microbial methane formation based on numerical reaction-transport modeling and a novel parameterization of Holocene sedimentation, *Geochim. Cosmochim. Acta*, *75*(16), 4562–4576, doi:10.1016/j.gca.2011.05.029.

Carslaw, H. S., and J. C. Jaeger (1959), *Conduction of Heat in Solids*, 2nd ed., Clarendon, Oxford, U. K.

Chylek, P., C. K. Folland, G. Lesins, M. K. Dubey, and M. Wang (2009), Arctic air temperature change amplification and the Atlantic Multidecadal Oscillation, *Geophys. Res. Lett.*, *36*, L14801, doi:10.1029/2009GL038777.

Dickson, R. R., T. J. Osborn, J. W. Hurrell, J. Meincke, J. Blindheim, B. Adlandsvik, T. Vinje, G. Alekseev, and W. Maslowski (2000), The Arctic Ocean response to the North Atlantic Oscillation, *J. Clim.*, *13*(15), 2671–2696, doi:10.1175/1520-0442(2000)013<2671:TAORTT>2.0.CO;2.

Faleide, J. I., S. T. Gudlaugsson, and G. Jacquart (1984), Evolution of the western Barents Sea, *Mar. Pet. Geol.*, *1*(2), 123–150, doi:10.1016/0264-8172(84)90082-5.

Fisher, R. E., et al. (2011), Arctic methane sources: Isotopic evidence for atmospheric inputs, *Geophys. Res. Lett.*, *38*, L21803, doi:10.1029/2011GL049319.

Ginsburg, G. D., and V. A. Soloviev (1995), Submarine gas hydrate estimation: Theoretical and empirical approaches, paper presented at Offshore Technology Conference, Soc. of Pet. Eng., Houston, Tex.

Graversen, R. G., T. Mauritsen, M. Tjernstrom, E. Kallen, and G. Svensson (2008), Vertical structure of recent Arctic warming, *Nature*, *451*(7174), 53–56, doi:10.1038/nature06502.

Haflidason, H., H. P. Sejrup, A. Nygård, J. Mienert, P. Bryn, R. Lien, C. F. Forsberg, K. Berg, and D. G. Masson (2004), The Storegga Slide: Architecture, geometry and slide development, *Mar. Geol.*, *213*, 201–234, doi:10.1016/j.margeo.2004.10.007.

Hansen, B., and S. Østerhus (2000), North Atlantic-Nordic Seas exchanges, *Prog. Oceanogr.*, *45*(2), 109–208, doi:10.1016/S0079-6611(99)00052-X.

Hansen, J., R. Ruedy, M. Sato, and K. Lo (2010), Global surface temperature change, *Rev. Geophys.*, *48*, RG4004, doi:10.1029/2010RG000345.

Harris, C. L., A. J. Plueddemann, and G. G. Gawarkiewicz (1998), Water mass distribution and polar front structure in the western Barents Sea, *J. Geophys. Res.*, *103*(C2), 2905–2917, doi:10.1029/97JC02790.

Harvey, L. D. D., and Z. Huang (1995), Evaluation of the potential impact of methane clathrate destabilization on future global warming, *J. Geophys. Res.*, *100*(D2), 2905–2926, doi:10.1029/94JD02829.

Haugan, P. M., G. Evensen, J. A. Johannessen, O. M. Johannessen, and L. H. Pettersson (1991), Modeled and observed mesoscale circulation and wave-current refraction during the 1988 Norwegian continental shelf experiment, *J. Geophys. Res.*, *96*(C6), 10,487–10,506, doi:10.1029/91JC00299.

Hegerl, G. C., F. W. Zwiers, P. Braconnot, N. P. Gillett, Y. Luo, J. A. Marengo Orsini, N. Nicholls, J. E. Peener, and P. A. Stott (2007), Understanding and attributing climate change, in *Climate Change 2007: The Physical Science Basis. Contribution of Working Group I to the Fourth Assessment Report of the Intergovernmental Panel on Climate Change*, edited by S. Solomon et al., pp. 663–745, Cambridge Univ. Press, New York.

Hurrell, J. W. (1995), Decadal trends in the North Atlantic Oscillation: Regional temperatures and precipitation, *Science*, *269*(5224), 676–679, doi:10.1126/science.269.5224.676.

Hurrell, J. W., Y. Kushnir, and M. Visbeck (2001), The North Atlantic Oscillation, *Science*, *291*(5504), 603–605, doi:10.1126/science.1058761.

Hustoft, S., B. Dugan, and J. Mienert (2009a), Effects of rapid sedimentation on developing the Nyegga pockmark field: Constraints from hydrological modeling and 3-D seismic data, offshore mid-Norway, *Geochem. Geophys. Geosyst.*, *10*, Q06012, doi:10.1029/2009GC002409.

Hustoft, S., S. Bünz, J. Mienert, and S. Chand (2009b), Gas hydrate reservoir and active methane-venting province in sediments on <20 Ma young oceanic crust in the Fram Strait, offshore NW-Svalbard, *Earth Planet. Sci. Lett.*, *284*(1–2), 12–24, doi:10.1016/j.epsl.2009.03.038.

Intergovernmental Panel on Climate Change (IPCC) (2007), *Climate Change 2007: The Physical Science Basis. Contribution of Working Group I to the Fourth Assessment Report of the Intergovernmental Panel on Climate Change*, edited by S. Solomon et al., Cambridge Univ. Press, New York.

Jain, P. C. (1993), Greenhouse effect and climate change: Scientific basis and overview, *Renew. Energy*, *3*(4–5), 403–420, doi:10.1016/0960-1481(93)90108-S.

Knies, J., E. Damm, J. Gutt, U. Mann, and L. Pinturier (2004), Near-surface hydrocarbon anomalies in shelf sediments off Spitsbergen: Evidences for past seepages, *Geochem. Geophys. Geosyst.*, *5*, Q06003, doi:10.1029/2003GC000687.

Krey, V., et al. (2009), Gas hydrates: Entrance to a methane age or climate threat?, *Environ. Res. Lett.*, *4*, 034007, doi:10.1088/1748-9326/4/3/034007.

Kvenvolden, K. (1988), Methane hydrate—A major reservoir of carbon in the shallow geosphere?, *Chem. Geol.*, *71*(1–3), 41–51, doi:10.1016/0009-2541(88)90104-0.

Kvenvolden, K. A. (1993), Gas hydrates-geological perspective and global change, *Rev. Geophys.*, *31*(2), 173–187, doi:10.1029/93RG00268.

MacDonald, G. J. (1990), Role of methane clathrates in past and future climates, *Clim. Change*, *16*(3), 247–281, doi:10.1007/BF00144504.

Midttomme, K., and E. Roaldset (2008), The effect of grain size on thermal conductivity of quartz sands and silts, *Pet. Geosci.*, *4*(2), 165–172, doi:10.1144/petgeo.4.2.165.

Mienert, J., and J. Posewang (1999), Evidence of shallow- and deep-water gas hydrate destabilizations in North Atlantic polar continental margin sediments, *Geo Mar. Lett.*, *19*(1), 143–149, doi:10.1007/s003670050101.

Mienert, J., and P. E. Weaver (2003), *European Margin Sediment Dynamics: Side-Scan Sonar and Seismic Images*, Springer, Berlin.

Mienert, J., J. Posewang, and M. Baumann (1998), Gas hydrates along the northeastern Atlantic margin: Possible hydrate-bound margin instabilities and possible release of methane, in *Gas Hydrates: Relevance to World Margin Stability and Climate Change*, edited by J.-P. Henriet and J. Mienert, *Geol. Soc. Spec. Publ.*, *137*, 275–291, doi:10.1144/GSL.SP.1998.137.01.22.

Mienert, J., M. Vanneste, S. Bünz, K. Andreassen, H. Haflidason, and H. P. Sejrup (2005), Ocean warming and gas hydrate stability on the mid-Norwegian margin at the Storegga Slide, *Mar. Pet. Geol.*, *22*, 233–244, doi:10.1016/j.marpetgeo.2004.10.018.

Milkov, A. V. (2004), Global estimates of hydrate-bound gas in marine sediments: How much is really out there?, *Earth Sci. Rev.*, *66*(3–4), 183–197, doi:10.1016/j.earscirev.2003.11.002.

Piechura, J., A. Beszczyńska-Möller, and R. Osiński (2001), Volume, heat and salt transport by the West Spitsbergen Current, *Polar Res.*, *20*(2), 233–240, doi:10.1111/j.1751-8369.2001.tb00061.x.

Rajan, A., J. Mienert, and S. Bünz (2012), Acoustic evidence for a gas migration and release system in Arctic glaciated continental margins offshore NW-Svalbard, *Mar. Pet. Geol.*, *32*, 36–49, doi:10.1016/j.marpetgeo.2011.12.008.

R Development Core Team (2010), *R: A Language and Environment for Statistical Computing*, R Found. for Stat. Comput., Vienna. [Available at http://www.R-project.org.]

Reagan, M. T., and G. J. Moridis (2009), Large-scale simulation of methane hydrate dissociation along the West Spitsbergen Margin, *Geophys. Res. Lett.*, *36*, L23612, doi:10.1029/2009GL041332.

Rignot, E., and P. Kanagaratnam (2006), Changes in the velocity structure of the Greenland ice sheet, *Science*, *311*(5763), 986–990, doi:10.1126/science.1121381.

Sætre, R. (1999), Features of the central Norwegian shelf circulation, *Cont. Shelf Res.*, *19*(14), 1809–1831, doi:10.1016/S0278-4343(99)00041-2.

Saunders, P. M. (1981), Practical conversion of pressure to depth, *J. Phys. Oceanogr.*, *11*, 573–574, doi:10.1175/1520-0485(1981)011<0573:PCOPTD>2.0.CO;2.

Schlichtholz, P., and I. Goszczko (2006), Interannual variability of the Atlantic water layer in the West Spitsbergen Current at 76.5°N in summer 1991–2003, *Deep Sea Res. Part I*, *53*(4), 608–626, doi:10.1016/j.dsr.2006.01.001.

Screen, J. A., and I. Simmonds (2010), The central role of diminishing sea ice in recent Arctic temperature amplification, *Nature*, *464*(7293), 1334–1337, doi:10.1038/nature09051.

Shakhova, N., I. Semiletov, A. Salyuk, V. Yusupov, D. Kosmach, and Ö. Gustafsson (2010), Extensive methane venting to the atmosphere from sediments of the East Siberian Arctic Shelf, *Science*, *327*(5970), 1246–1250, doi:10.1126/science.1182221.

Shipley, T. H., M. H. Houston, R. T. Buffler, F. J. Shaub, K. J. McMillen, J. W. Ladd, and J. L. Worzel (1979), Seismic reflection evidence for widespread occurrence of possible gas-hydrate horizons on continental slopes and rises, *Am. Assoc. Pet. Geol. Bull.*, *63*, 2204–2213.

Sidorova, A., and A. Shcherbinin (2009), Barents Sea hydrodynamics change during the El Niño event, *Dokl. Earth Sci.*, *429*(2), 1562–1566, doi:10.1134/S1028334X09090311.

Sloan, E. D. J. (1990), *Clathrate Hydrates of Natural Gases*, 641 pp., Marcel Dekker, New York.

Sloan, E. D. J. (1998), Physical/chemical properties of gas hydrates and application to world margin stability and climatic change, in *Gas Hydrates, Relevance to World Margin Stability and Climatic Change*, edited by J.-P. H. J. Mienert, pp. 31–50, Geol. Soc., London, doi:10.1144/GSL.SP.1998.137.01.03.

Solheim, A., and A. Elverhøi (1985), A pockmark field in the Central Barents Sea; Gas from a petrogenic source?, *Polar Res.*, *3*(1), 11–19, doi:10.1111/j.1751-8369.1985.tb00492.x.

Spielhagen, R. F., K. Werner, S. A. Sørensen, K. Zamelczyk, E. Kandiano, G. Budeus, K. Husum, T. M. Marchitto, and M. Hald (2011), Enhanced modern heat transfer to the Arctic by warm Atlantic water, *Science*, *331*(6016), 450–453, doi:10.1126/science.1197397.

Stenseth, N. C., G. Ottersen, J. W. Hurrell, A. Mysterud, M. Lima, K. S. Chan, N. G. Yoccoz, and B. Ådlandsvik (2003), Studying climate effects on ecology through the use of climate indices: The North Atlantic Oscillation, El Niño Southern Oscillation and beyond, *Proc. R. Soc. London Ser. B*, *270*(1529), 2087–2096, doi:10.1098/rspb.2003.2415.

Swift, J. H., and K. Aagaard (1981), Seasonal transitions and water mass formation in the Iceland and Greenland seas, *Deep Sea Res. Part A*, *28*(10), 1107–1129, doi:10.1016/0198-0149(81)90050-9.

Tishchenko, P., Hensen, C., Wallmann, K., and C. S. Wong (2005), Calculation of the stability and solubility of methane hydrate in seawater, *Chem. Geol.*, *219*, 37–52, doi:10.1016/j.chemgeo.2005.02.008.

Turpeinen, H., A. Hampel, T. Karow, and G. Maniatis (2008), Effect of ice sheet growth and melting on the slip evolution of thrust faults, *Earth Planet. Sci. Lett.*, *269*(1–2), 230–241, doi:10.1016/j.epsl.2008.02.017.

Vanneste, M., S. Guidard, and J. Mienert (2005), Arctic gas hydrate provinces along the western Svalbard continental margin, in *Proceedings of the Norwegian Petroleum Society Conference*, *Norw. Pet. Soc. Spec. Publ.*, *12*, 271–284, doi:10.1016/S0928-8937(05)80054-2.

Vinther, B. M., et al. (2009), Holocene thinning of the Greenland ice sheet, *Nature*, *461*(7262), 385–388, doi:10.1038/nature08355.

Vogt, P. R., and E. Sundvor (1996), Heat flow highs on the Norwegian-Barents-Svalbard continental slope: Deep crustal fractures, dewatering or "memory in the mud," *Geophys. Res. Lett.*, *23*(24), 3571–3574, doi:10.1029/96GL03259.

Vogt, P. R., K. Crane, E. Sundvor, M. D. Max, and S. L. Pfirman (1994), Methane-generated(?) pockmarks on young, thickly sedimented oceanic crust in the Arctic: Vestnesa ridge, Fram strait, *Geology*, *22*(3), 255–258, doi:10.1130/0091-7613(1994)022<0255:MGPOYT>2.3.CO;2.

Vogt, P. R., J. Gardner, and K. Crane (1999), The Norwegian-Barents-Svalbard (NBS) continental margin: Introducing a natural laboratory of mass wasting, hydrates, and ascent of sediment, pore water, and methane, *Geo Mar. Lett.*, *19*(1), 2–21, doi:10.1007/s003670050088.

Von Herzen, R. P., and A. E. Maxwell (1959), The measurement of thermal conductivity of deep-sea sediments by a needle-probe method, *J. Geophys. Res.*, *64*, 1557–1563, doi:10.1029/JZ064i010p01557.

Vorren, T. O., J. S. Laberg, F. Blaume, J. A. Dowdeswells, N. H. Kenyon, J. Mienert, J. Rumohr, and F. Werner (1998), The Norwegian-Greenland Sea continental margins: Morphology and late quaternary sedimentary processes and environment, *Quat. Sci. Rev.*, *17*, 273–302, doi:10.1016/S0277-3791(97)00072-3.

Westbrook, G. K., et al. (2009), Escape of methane gas from the seabed along the West Spitsbergen continental margin, *Geophys. Res. Lett.*, *36*, L15608, doi:10.1029/2009GL039191.